Work published on IEEE Trans. on Instrumentation and Measurement, 64(12),7271041, pp. 3284-3296, 2015,
DOI 10.1109/TIM.2015.2469433.

Low-complexity Least Squares Dynamic Synchrophasor Estimation based on the Discrete Fourier Transform

Daniel Belega[1], *Member, IEEE,* Daniele Fontanelli[2], *Member, IEEE,* Dario Petri[2], *Fellow, IEEE*

[1]Department of Measurements and Optical Electronics,
Politehnica University Timişoara, Timişoara, Romania,
E-mail: *daniel.belega@upt.ro*

[2]Department of Industrial Engineering,
University of Trento, Trento, Italy,
E-mail: *daniele.fontanelli@unitn.it*, *dario.petri@unitn.it*

Abstract *— In this paper the expressions for the phasor parameter estimates returned by the Taylor-based Weighted Least Square (TWLS) approach, achieved using either complex-valued or real-valued variables, are derived. In particular, the TWLS phasor estimator and its derivatives are expressed as weighted sums of the Discrete Time Fourier Transform (DTFT) of the analyzed waveform and its derivatives. The derived expressions show that the TWLS algorithm is sensitive to lower order harmonics and inter-harmonics located close to the waveform frequency when few waveform cycles are analyzed. Also, the algorithm sensitivity to wideband noise is explained. The relationship between the TWLS phasor estimator and the waveform DTFT is then specifically analyzed when either a static or a second-order dynamic phasor model is assumed. Moreover, a simple and accurate procedure for evaluating the TWLS estimator of the dynamic phasor parameters is proposed. The derived expressions for the real-valued version are then approximated in order to reduce the required computational burden so achieving the Simplified TWLS (STWLS) procedure. That procedure can be advantageously employed in real-time low-cost applications when the reference frequency used in the TWLS approach is estimated run-time to improve estimation accuracy. Finally, computer simulations show that the phasor parameter estimates returned by the STWLS procedure when the waveform frequency is estimated by the Interpolated Discrete Fourier Transform method comply with the M-class of performance if an appropriate number of waveform cycles is considered.*

Index terms *— Dynamic phasor estimation, power system monitoring, Taylor-based weighted least squares algorithm, Discrete Fourier Transform, windowing.*

I. INTRODUCTION

Phasor parameters of electrical waveforms are increasingly employed in power grids for monitoring, control, and protection purposes. Smart devices called Phasor Measurement Units (PMUs) use different algorithms to provide accurate measurements of waveform phasor, frequency, and Rate Of Change Of Frequency (ROCOF) at instants synchronized with the Coordinated Universal Time (UTC). The performance requirements of PMUs have been specified in the IEEE Standard C37.118.1-2011 about synchrophasor measurements for power systems [1], recently updated in the Amendment IEEE Standard C37.118.1a-2014 [2]. In these two documents (simply referred to as the Standard for the sake of notation) the phasor measurement accuracy is defined in terms of the Total Vector Error (*TVE*), the Frequency Error (*FE*), and the ROCOF Error (*RFE*). Recently, algorithms based on either a dynamic phasor model [3]-[17] or a static model [18]-[20] have been proposed to estimate these parameters. Indeed, power waveform parameters may be affected by time variations and algorithms that adopt a dynamic phasor model may provide more accurate estimates, especially when the observed waveform length is more than a couple of cycles. In particular, the so-called Taylor-based Weighted Least Squares (TWLS) algorithm [5], [6] is capable of providing not only phasor measurements, but also Frequency Deviation (*FD*) and *ROCOF* estimates [5], [12]. The classical TWLS algorithm considers complex-valued data, but a real-valued version has been recently proposed [21]. Moreover, it has been shown that accurate phasor parameter estimates usually need a reference frequency quite close to the waveform frequency [11], [17]. This requires runtime frequency estimation and a significant increase in the computational burden of the TWLS phasor parameter estimator due to the derivation of the related pseudoinverse matrix. In this respect, the real-valued TWLS algorithm exhibits a higher processing efficiency [21]. In order to minimize the required processing effort, *a-priori* computation and subsequent storage of pseudoinverse matrices related to different values of the reference frequency have been proposed [11], [17]. It has been shown that limiting to integer frequency values allow to achieve satisfactory estimation accuracy, even though this approach requires a significant use of storage when the number of observed waveform cycles cannot be small as occurs when a good inter-harmonics rejection is required [17]. At the best of the authors' knowledge, no processing procedure has been yet proposed in the scientific literature to avoid runtime computation of the pseudoinverse matrix when estimating phasor parameters by the TWLS algorithm.

Another accurate dynamic phasor parameter estimator based on Discrete Fourier Transform (DFT) samples has been recently proposed [15]. However, despite the close link between the TWLS approach and the Fourier transform is well-known [5], [6], the relationship between the TWLS estimator of the dynamic phasor parameters and the Discrete Time Fourier Transform (DTFT) of the analyzed waveform has not yet been published in the scientific literature. This relationship is of interest because it would allow a better

understanding of the effect on estimation accuracy of some disturbance components superimposed to the sinewave waveform, such as harmonics, inter-harmonics, and wideband noise. Moreover, this relationship could suggest different procedures for the evaluation of the TWLS phasor estimator. Therefore, the aim of this paper is twofold: at first linking the phasor parameter estimates provided by the TWLS algorithm and the DTFT of the analyzed waveform, then using the obtained expressions to derive a procedure that implement the TWLS algorithm without computing the matrix pseudoinverse.

The remainder of the paper is organized as follows. Section II briefly summarizes both the complex-valued and the real-valued version of the TWLS estimation approach. In Section III the relationship between the TWLS estimator of the dynamic phasor parameters and the DTFT of the analyzed waveform is derived. The achieved expressions enable us to explain the effect on estimated phasor parameters of disturbances like harmonics, inter-harmonics, and additive wideband noise. Also, two phasor models widely adopted in the literature, i.e., the static phasor and the second-order dynamic phasor are specifically considered. The expressions obtained in this latter case for the real-valued version of the algorithm are then approximated in order to reduce the required computational effort so achieving the Simplified TWLS (STWLS) procedure. In Section IV it is shown that the phasor parameter estimates returned by the STWLS procedure when the waveform frequency is estimated by the Interpolated Discrete Fourier Transform (IpDFT) method (i.e. the STWLS-IpDFT procedure) comply with the requirements of the *M-class* of performance when an appropriate number of waveform cycles is considered. Moreover, the accuracies of the phasor parameter estimates provided by the STWLS procedure are analyzed when the coefficients involved in the derived expressions are evaluated by means of simple polynomials. The computation burden required by the considered TWLS procedures is also discussed. Finally, Section V concludes the paper.

II. COMPLEX-VALUED AND REAL-VALUED TWLS APPROACHES

The analyzed electrical waveform is modeled as:

$$x(t) = a(t)\cos(2\pi f_0 t + \varphi(t)) = \mathrm{Re}\left\{p(t)e^{j2\pi f_0 t}\right\} = \frac{1}{2}\left(p(t)e^{j2\pi f_0 t} + p^*(t)e^{-j2\pi f_0 t}\right), \tag{1}$$

where $p(t) = a(t)e^{j\varphi(t)}$, is the so-called complex dynamic phasor of the waveform $x(\cdot)$ synchronized to the reference frequency f_0, and $\mathrm{Re}\{\cdot\}$ denotes the real part of its argument. The components of the phasor $p(t)$ are the time-varying amplitude and angle $a(t)$ and $\varphi(t)$, respectively. It is worth noticing that when f_0 is equal to the nominal frequency f_n (50 Hz or 60 Hz), the phasor $p(t)$ is simply called the synchrophasor.

The analyzed discrete-time waveform is achieved by sampling the continuous-time waveform (1) using a sampling rate f_s synchronized with the UTC. It is assumed that the following relationship holds for the nominal normalized frequency ν_n:

$$\nu_n = \frac{f_n}{f_s} = \frac{J}{M-1}, \tag{2}$$

where J is integer and represents the number of analyzed nominal waveform cycles and $M = 2N_H + 1$ represents the odd number of analyzed samples. Also, the number of samples per nominal cycle $N = f_s/f_n$ is integer and the reference time $t_r = r/f_s$, $r = 0, 1, 2,...$ is located exactly at the center of the r-th record of data, whose duration is $T = M/f_s$.

In the following of this section the well-known complex-valued TWLS phasor estimator is briefly described, together with the most recent real-valued TWLS approach [21].

A. *Complex-valued TWLS approach*

According to the complex-valued approach the phasor $p(t)$ is expressed by using its complex Taylor's series about the reference time t_r, $r = 0, 1,2,...$, truncated to the Kth order term, i.e.,

$$p(t) \cong p(t_r) + p'(t_r)\Delta t + \frac{p''(t_r)}{2!}\Delta^2 t + \ldots + \frac{p^{(K)}(t_r)}{K!}\Delta^K t, \qquad |\Delta t| \le \tfrac{1}{2}T \tag{3}$$

where $\Delta t = t - t_r$, $p^{(k)}(t_r)$, $k = 1, 2,..., K$, is the k-th order derivative of $p(t)$ computed at the reference time t_r. The coefficients of the Taylor's polynomial (3) are then estimated as [6]:

$$\hat{P}_{K,r}^{(C)} = 2\left(Q_K^H W^H W Q_K\right)^{-1} Q_K^H W^H W x_r = A_K^{-1} C_K x_r, \quad r = 0,1,2,\ldots \tag{4}$$

where

$$\hat{P}_{K,r}^{(C)} = \left[\hat{p}_{K,r}^{(C)}\ \hat{p}_{K-1,r}^{(C)} \ldots \hat{p}_{1,r}^{(C)}\ \hat{p}_{0,r}^{(C)}\ \hat{p}_{0,r}^{(C)*}\ \hat{p}_{1,r}^{(C)*} \ldots \hat{p}_{K-1,r}^{(C)*}\ \hat{p}_{K,r}^{(C)*}\right]^T, \tag{5}$$

with $p(t_r) = p_{0,r}^{(C)}$ and $p^{(k)}(t_r) = \left(k!\, f_s^{\,k}\right) p_{k,r}^{(C)}$, $k = 1,2,\ldots,K$; Q_K is a matrix of dimension $M\times(2K + 2)$, with elements q_{lh}, defined as:

$$Q_K = \begin{bmatrix} Q_{K,1} & Q_{K,3} \\ Q_{K,2} & Q_{K,4} \end{bmatrix}, \tag{6}$$

with entries:

$$
\begin{aligned}
\left(q_{K,1}\right)_{lh} &= \left(l-\frac{M+1}{2}\right)^{K+1-h} e^{-j2\pi\nu_0\left(\frac{M+1}{2}-l\right)}, \quad l=1,\ldots,\frac{M+1}{2} \text{ and } h=1,\ldots,K+1,\\
\left(q_{K,2}\right)_{lh} &= l^{K+1-h} e^{j2\pi\nu_0 l}, \qquad\qquad l=1,\ldots,\frac{M-1}{2} \text{ and } h=1,\ldots,K+1,\\
\left(q_{K,3}\right)_{lh} &= \left(l-\frac{M+1}{2}\right)^{h-1} e^{j2\pi\nu_0\left(\frac{M+1}{2}-l\right)}, \quad l=1,\ldots,\frac{M+1}{2} \text{ and } h=1,\ldots,K+1,\\
\left(q_{K,4}\right)_{lh} &= l^{h-1} e^{-j2\pi\nu_0 l}, \qquad\qquad l=1,\ldots,\frac{M-1}{2} \text{ and } h=1,\ldots,K+1
\end{aligned}
\tag{7}
$$

$\nu_0 = f_0/f_s$ is the normalized reference frequency, $x_r = [x(-N_H + r)\ldots x(r)\ldots x(N_H + r)]^T$ is the vector of the observed data, and $W = diag\left[w(-N_H)\, w(-N_H + 1)\ldots w(0)\ldots w(N_H - 1)\, w(N_H)\right]$ is the diagonal matrix formed by the samples of the adopted window $w(\cdot)$. Finally $A_K = \frac{1}{2} Q_K^H W^H W Q_K$ represents the Gram's matrix and $C_K = Q_K^H W^H W$. In the above expressions, $(\cdot)^*$, $(\cdot)^H$, and $(\cdot)^T$ denotes the conjugation, Hermitian, and transposition operators, respectively.

B. *Real-valued TWLS approach*

The waveform (1) can be rewritten as:

$$x(t) = c(t)\cos(2\pi f_0 t) - s(t)\sin(2\pi f_0 t), \tag{8}$$

in which $c(t) = a(t)\cos(\varphi(t))$ and $s(t) = a(t)\sin(\varphi(t))$. These two waveforms are expanded by using Taylor's series about the reference time t_r, $r = 0, 1,2,...$, truncated to the K-order terms, i.e.:

$$c(t) \cong c(t_r) + c'(t_r)\Delta t + \frac{c''(t_r)}{2!}\Delta^2 t + \ldots + \frac{c^{(K)}(t_r)}{K!}\Delta^K t, \tag{9.a}$$

and

$$s(t) \cong s(t_r) + s'(t_r)\Delta t + \frac{s''(t_r)}{2!}\Delta^2 t + \ldots + \frac{s^{(K)}(t_r)}{K!}\Delta^K t, \tag{9.b}$$

where $c^{(k)}(t_r)$ and $s^{(k)}(t_r)$, k = 1, 2,..., K, are the k-th order derivative of $c(t)$ and $s(t)$, respectively, computed at the reference time t_r. The coefficients of the Taylor's polynomials (9) are then estimated as [21]:

$$\hat{P}_{K,r}^{(R)} = \left(U_K^T W^T W U_K\right)^{-1} U_K^T W^T W x_r = B_K^{-1} D_K x_r, \quad r = 0,1,2,\ldots \tag{10}$$

where

$$\hat{P}_{K,r}^{(R)} = \left[\hat{c}_{K,r}\, \hat{c}_{K-1,r}\ldots\hat{c}_{1,r}\, \hat{c}_{0,r} - \hat{s}_{0,r} - \hat{s}_{1,r}\ldots - \hat{s}_{K-1,r} - \hat{s}_{K,r}\right]^T, \tag{11}$$

in which $c(t_r) = c_{0,r}$, $s(t_r) = s_{0,r}$, $c^{(k)}(t_r) = \left(k!\, f_s^{\,k}\right) c_{k,r}$, and $s^{(k)}(t_r) = \left(k!\, f_s^{\,k}\right) s_{k,r}$, $k = 1,2,\ldots,K$; U_K is a matrix of dimension $M\times(2K + 2)$, with elements u_{lh}, defined as [21]:

$$U_K = \begin{bmatrix} U_{K,1} & U_{K,3} \\ U_{K,2} & U_{K,4} \end{bmatrix}, \tag{12}$$

with entries:

$$\begin{aligned}
\left(u_{K,1}\right)_{lh} &= \left(l - \frac{M+1}{2}\right)^{K+1-h} \cos\left(2\pi\nu_0\left(\frac{M+1}{2} - l\right)\right), \quad l = 1,\ldots,\frac{M+1}{2} \text{ and } h = 1,\ldots,K+1, \\
\left(u_{K,2}\right)_{lh} &= l^{K+1-h}\cos(2\pi\nu_0 l), \qquad\qquad l = 1,\ldots,\frac{M-1}{2} \text{ and } h = 1,\ldots,K+1, \\
\left(u_{K,3}\right)_{lh} &= -\left(l - \frac{M+1}{2}\right)^{h-1} \sin\left(2\pi\nu_0\left(\frac{M+1}{2} - l\right)\right), \quad l = 1,\ldots,\frac{M+1}{2} \text{ and } h = 1,\ldots,K+1, \\
\left(u_{K,4}\right)_{lh} &= l^{h-1}\sin(2\pi\nu_0 l), \qquad\qquad l = 1,\ldots,\frac{M-1}{2} \text{ and } h = 1,\ldots,K+1
\end{aligned} \tag{13}$$

Moreover $B_K = U_K^T W^T W U_K$ is the Gram matrix and $D_K = U_K^T W^T W$. According to (8) and (9), the waveform phasor and its derivatives are then obtained as:

$$\hat{p}_{k,r}^{(R)} = \hat{c}_{k,r} + j\hat{s}_{k,r}, \quad k = 0,1,\ldots,K. \tag{14}$$

It can be shown that $\hat{p}_{k,r}^{(C)} = \hat{p}_{k,r}^{(R)} = \hat{p}_{k,r}$ $k = 0,1,\ldots,K$ [21] (see the Appendix A). Thus, no distinction between the phasor estimates returned by the two different approaches will be made in the remaining of the paper.

It is also worth noticing that the pseudoinverse matrices (i.e. $A_K^{-1}C_K$ or $B_K^{-1}D_K$ for the complex-valued or the real-valued versions, respectively) can be calculated off-line only once when the reference frequency is known *a-priori*. However, when the reference frequency is estimated at run-time to improve estimation accuracy [17], the computation of the pseudo-inverse matrix can require a relevant computational burden.

C. *Estimates of the phasor parameters*

The phasor amplitude and angle can be estimated respectively as [21]:

$$\hat{a}_x(t_r) = \left|\hat{p}_{0,r}\right|, \qquad \hat{\varphi}_x(t_r) = angle(\hat{p}_{0,r}), \tag{15}$$

the Frequency Deviation (*FD*) between the frequency *f* of the electrical waveform at the instant t_r and the reference frequency, i.e. $FD = f - f_0$, can be estimated as [21]:

$$\hat{FD}(t_r) = \frac{f_s}{2\pi}\frac{\mathrm{Im}\left\{\hat{p}_{1,r}\ \hat{p}_{0,r}^{*}\right\}}{\left|\hat{p}_{0,r}\right|^2}, \tag{16}$$

and the waveform Rate Of Change Of Frequency (ROCOF) is estimated as [21]:

$$\hat{ROCOF}(t_r) = \frac{f_s^2}{\pi}\left[\frac{\mathrm{Im}\left\{\hat{p}_{2,r}\ \hat{p}_{0,r}^*\right\}}{\left|\hat{p}_{0,r}\right|^2} - \frac{\mathrm{Re}\left\{\hat{p}_{1,r}\ \hat{p}_{0,r}^*\right\}\mathrm{Im}\left\{\hat{p}_{1,r}\ \hat{p}_{0,r}^*\right\}}{\left|\hat{p}_{0,r}\right|^4}\right], \tag{17}$$

According to the Standard [1], the related estimation accuracy parameters are defined as, the Total Vector Error (*TVE*):

$$TVE(t_r) = \frac{\left|\hat{a}_x(t_r)e^{j\hat{\varphi}_x(t_r)} - a(t_r)e^{j\varphi(t_r)}\right|}{\left|a(t_r)\right|}, \tag{18}$$

the Frequency Error (*FE*):

$$FE(t_r) = \left|\hat{FD}_x(t_r) - FD(t_r)\right|, \tag{19}$$

and the ROCOF Error (*RFE*):

$$RFE(t_r) = \left|\hat{ROCOF}(t_r) - ROCOF(t_r)\right|. \tag{20}$$

III. RELATIONSHIP BETWEEN THE TWLS PHASOR ESTIMATOR AND THE WAVEFORM DTFT

The estimate of the phasor parameters returned by the real-valued TWLS approach can be expressed as (see (B.10) in the Appendix B):

$$\begin{aligned}\hat{p}_{K-k,r}^{(R)} = \hat{c}_{K-k,r} + j\hat{s}_{K-k,r} = &\sum_{l=1}^{K+1}\left[\beta_{(k+1)l} - j\beta_{(2K+2-k)l}\right]\mathrm{Re}\left\{\left(\frac{j}{2\pi}\right)^{K+1-l} X_{W_2}^{(K+1-l)}(\nu_0)\right\} \\ &+ j\sum_{l=1}^{K+1}\left[\beta_{(2K+2-k)(2K+3-l)} + j\beta_{(k+1)(2K+3-l)}\right]\mathrm{Im}\left\{\left(\frac{j}{2\pi}\right)^{K+1-l} X_{W_2}^{(K+1-l)}(\nu_0)\right\}, \qquad k = 0,1,\ldots,K\end{aligned} \tag{21}$$

where β_{lh}, l, h = 1, 2,…, 2K + 2, are the elements of the inverse matrix $B_K^{-1} = \left(U_K^H W^H W U_K\right)^{-1}$, $X_{W_2}(\cdot)$ is the DTFT of the analyzed waveform weighted by the square window $w^2(\cdot)$ and $X_{W_2}^{(k)}(\cdot)$ is its k-order derivative, k = 0, 1, 2,…, K.

A very similar relationship can be achieved when considering the complex-valued TWLS approach:

$$\hat{p}_{K-k,r}^{(C)} = 2\sum_{l=1}^{K+1}\alpha_{(k+1)l}\left(\frac{j}{2\pi}\right)^{K+1-l} X_{W_2}^{(K+1-l)}(\nu_0) + 2\sum_{l=1}^{K+1}\alpha_{(k+1)(2K+3-l)}\left(\frac{j}{2\pi}\right)^{K+1-l} X_{W_2}^{(K+1-l)*}(\nu_0), \quad k = 0,1,\ldots,K, \tag{22}$$

in which α_{lh}, l, h = 1, 2,…, 2K + 2 are the elements of the inverse matrix $\frac{1}{2}A_K^{-1} = \left(Q_K^H W^H W Q_K\right)^{-1}$ and can be easily expressed in terms of the coefficients β_{lh}, l, h = 1, 2,…, 2K + 2 introduced in (21).

Expressions (21) and (22) show that the estimates of the phasor parameters returned by the TWLS approach are weighted sums of $X_{W_2}^{(k)}(\cdot)$. Moreover, the coefficients α_{lh} and β_{lh} depend on the DTFT of the square window $w^2(\cdot)$, $W_2(\cdot)$ and its derivatives $W_2^{(k)}(\cdot)$, k = 0, 1,…, K (see (B.5) and (B.6) in the Appendix B).

It can be easily proved that the square window $w^2(\cdot)$ of a H-term cosine window $w(\cdot)$ ($H \geq 2$) is a (2H - 1)–term cosine window. In particular, the 2k-power order of the two-term Maximum Sidelobe Decay (MSD) (or Hann) window [22] is the (2k +1)-term MSD window. Fig. 1 shows the DTFT spectra of the Hann window, the related square window $w^2(\cdot)$ (i.e., the three-term MSD window) and its first and second derivatives versus the normalized frequency expressed in bins $\lambda = (M - 1)\nu$. Indeed, this choice for the abscissa allows us to obtain a window sidelobe spectrum behavior almost independent of the number of observed samples M, at least for the mainlobe and the first sidelobes. The spectra are expressed in dB with respect to their maximum value, which occurs at λ = 0 for the window and square window transforms $W(\cdot)$ and $W_2(\cdot)$, respectively. Conversely, for the first derivative $W_2^{(1)}(\cdot)$ the maximum of the spectrum is almost proportional to the number of analyzed samples M and it occurs when λ is close to 2. Conversely, the maximum is almost proportional to M^2 for the second derivative $W_2^{(2)}(\cdot)$ and it occurs at λ = 0 (see (B.5) and (B.6) in the Appendix B).

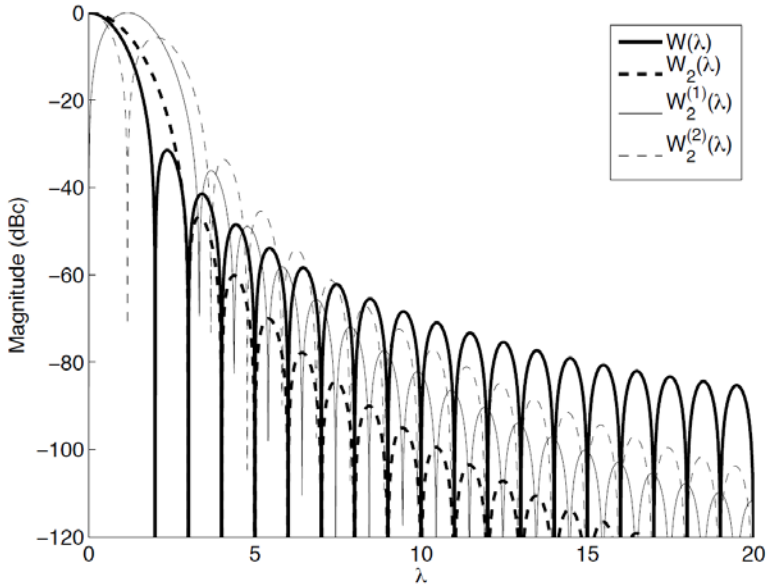

Fig. 1. Spectra of the DTFT of the Hann window $w(\cdot)$, the related square window $w^2(\cdot)$, and its first and second derivatives versus λ. Number of sample per nominal cycle N = 24, observation interval length J = 2.

Fig. 1 shows that, for small values of λ, the spectrum of the square window and its first and second derivatives are more spread than the Hann window. In particular, the spectrum side-lobe level increases as the derivative order increases. In addition, unlike $W(\cdot)$ and $W_2(\cdot)$, $W_2^{(1)}(\cdot)$ and $W_2^{(2)}(\cdot)$ are not null at integer values of λ. Similar behaviors can be shown for any other classical cosine window [22]. As a consequence, the following remarks about estimates returned by the TWLS algorithm can be drawn:

- when a low number of waveform cycles is analyzed (e.g. one or two cycles), the sensitivity of the TWLS algorithm to lower order harmonics and inter-harmonics located close to the waveform frequency is expected to be higher than a DTFT approach based on the same window $w(\cdot)$; indeed, the spectra of the square window and its derivatives generally exhibit a stronger short-range leakage;
- when an integer number of waveform cycles is analyzed (i.e. coherent sampling occurs), the contribution of harmonics to the estimated phasor parameters is not null since the spectra of the window derivatives $W_2^{(k)}(\cdot)$, $k = 1, 2, \ldots, K$ are not null at the related frequencies;
- the sensitivity of the TWLS algorithm to wideband noise is expected to be higher than the DTFT approach based on the same window $w(\cdot)$ due to the higher Equivalent Noise BandWidth (ENBW) of the square window and its derivatives [23].

The above remarks are corroborated by computer simulations reported in several recently published papers, such as [5], [6], [10], [13], and [17].

In the following, the results returned by (21) and (22) are analyzed for two specific phasor models widely adopted in the scientific literature: the static phasor model (i.e. $K = 0$) and the second-order dynamic phasor model (i.e. $K = 2$, which is the minimum Taylor's series order allowing the estimation of the phasor amplitude and angle, frequency deviation, and ROCOF).

A. *Static phasor model* ($K = 0$)

Assuming a static phasor model, that is $K = 0$ in (3), the TWLS approach reduces to the well-known three-parameter sine-fitting algorithm when applied in the special case of zero offset [24]. In this case both (21) and (22) provide (see (B.15) in the Appendix B):

$$\hat{p}_{0,r} = 2\frac{W_2(0)\,X_{W_2}(\nu_0) - W_2(2\nu_0)\,X^*_{W_2}(\nu_0)}{W_2^2(0) - W_2^2(2\nu_0)}, \tag{23}$$

where $\nu_0 = f_0/f_s$.

If the reference frequency corresponds to an integer number of observed cycles (i.e. ν_0 is integer), as often occurs in practice, and a classical cosine window is employed, than $W_2(2\nu_0) = 0$, and (23) simply becomes:

$$\hat{p}_{0,r} = \frac{2}{W_2(0)} X_{W_2}(\nu_0), \tag{24}$$

which shows that the TWLS method is equivalent to the simple DFT estimator based on the square window $w^2(\cdot)$.

B. *Second order dynamic phasor model* ($K = 2$)

The analytical relationship for the phasor parameters when $K = 2$ can be obtained from (4) or (10) by inverting the 6x6 matrices $A_K = \frac{1}{2} Q_K^H W^H W Q_K$ or $B_K = U_K^T W^T W U_K$, respectively. The expressions for the entries of the inverse matrices have been determined by means of the *Symbolic Math Toolbox* of MATLAB. It was observed that A_K^{-1} is a Hankel matrix, but expressions returning the values of its entries as a function of the adopted window are very complicated (each one has more than 50 terms). Conversely, the matrix B_K^{-1} is a symmetric Hankel matrix with only 12 different not-null entries β_{11}, β_{13}, β_{15}, β_{22}, β_{24}, β_{26}, β_{33}, β_{35}, β_{44}, β_{46}, β_{55}, and β_{66}, expressed in a quite simple way as a function of the adopted window samples, and 18 null elements (see (B.18) and (B.19) in the Appendix B). Thus, the analytical relationships that link the second-order TWLS estimator of the phasor parameters and the DTFT of the analyzed waveform are:

$$\begin{aligned}
\hat{c}_{0,r} &= \beta_{33} \operatorname{Re}\{X_{W_2}(\nu_0)\} - \frac{\beta_{35}}{2\pi} \operatorname{Re}\left\{X_{W_2}^{(1)}(\nu_0)\right\} - \frac{\beta_{13}}{4\pi^2} \operatorname{Re}\left\{X_{W_2}^{(2)}(\nu_0)\right\}, \\
\hat{s}_{0,r} &= \beta_{44} \operatorname{Im}\{X_{W_2}(\nu_0)\} + \frac{\beta_{24}}{2\pi} \operatorname{Im}\left\{X_{W_2}^{(1)}(\nu_0)\right\} - \frac{\beta_{46}}{4\pi^2} \operatorname{Im}\left\{X_{W_2}^{(2)}(\nu_0)\right\}, \\
\hat{c}_{1,r} &= -\beta_{24} \operatorname{Im}\{X_{W_2}(\nu_0)\} - \frac{\beta_{22}}{2\pi} \operatorname{Im}\left\{X_{W_2}^{(1)}(\nu_0)\right\} + \frac{\beta_{26}}{4\pi^2} \operatorname{Im}\left\{X_{W_2}^{(2)}(\nu_0)\right\}, \\
\hat{s}_{1,r} &= -\beta_{35} \operatorname{Re}\{X_{W_2}(\nu_0)\} + \frac{\beta_{55}}{2\pi} \operatorname{Re}\left\{X_{W_2}^{(1)}(\nu_0)\right\} + \frac{\beta_{15}}{4\pi^2} \operatorname{Re}\left\{X_{W_2}^{(2)}(\nu_0)\right\}, \\
\hat{c}_{2,r} &= \beta_{13} \operatorname{Re}\{X_{W_2}(\nu_0)\} - \frac{\beta_{15}}{2\pi} \operatorname{Re}\left\{X_{W_2}^{(1)}(\nu_0)\right\} - \frac{\beta_{11}}{4\pi^2} \operatorname{Re}\left\{X_{W_2}^{(2)}(\nu_0)\right\}, \\
\hat{s}_{2,r} &= \beta_{46} \operatorname{Im}\{X_{W_2}(\nu_0)\} + \frac{\beta_{26}}{2\pi} \operatorname{Im}\left\{X_{W_2}^{(1)}(\nu_0)\right\} - \frac{\beta_{66}}{4\pi^2} \operatorname{Im}\left\{X_{W_2}^{(2)}(\nu_0)\right\}.
\end{aligned} \tag{25}$$

The behaviors of the not null coefficients of the matrix B_2^{-1} versus the reference frequency employed in the algorithm are reported in Fig. 2 when the Hann window is adopted and $M = 49$ samples (i.e. $J = 2$ waveform cycles) (Fig. 2(a)) and $M = 97$ (i.e. $J = 4$ cycles) (Fig. 2(b)) are analyzed. It is worth noticing that the reference frequency $\lambda_0 = (M - 1)\nu_0$ is expressed in bins in order to obtain similar curves for different values of M.

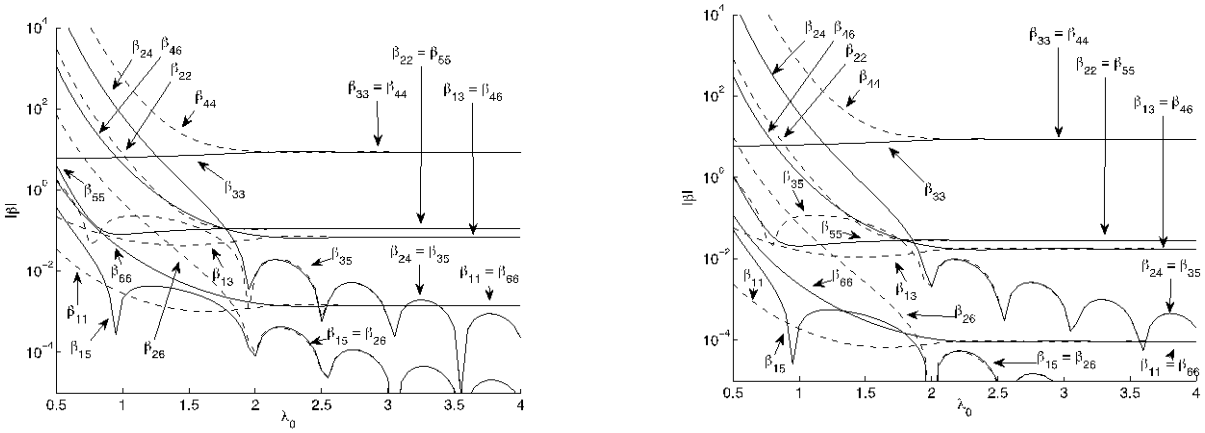

(a) (b)

Fig. 2. Behavior of the not null entries β_{ij} of the inverse matrix B_2^{-1} used in (10) versus $\lambda_0 = (M - 1)\nu_0$ for the Hann window assuming (a) $M = 49$ ($J = 2$ cycles) and (b) $M = 97$ ($J = 4$ cycles).

As expected (see the Appendix B), Fig. 2 shows that when λ_0 is greater than 2-3 bins (obviously λ_0 must be lower than $(M - 1)/2$ to avoid aliasing) we have: $\beta_{26} \cong \beta_{15}$, $\beta_{35} \cong \beta_{24}$, $\beta_{44} \cong \beta_{33}$, $\beta_{46} \cong \beta_{13}$, $\beta_{55} \cong \beta_{22}$, and $\beta_{66} \cong \beta_{11}$. Also, the most relevant couples are almost independent of λ_0 and the difference between the related couples of elements decreases as λ_0 increases.

Behaviors very similar to those reported in Fig. 2 were observed when considering different windows and number of samples.

Observe also that the asymptotic (large values of λ_0) values of the coefficients β_{lh} depend on the number of acquired samples M. In particular, it can be shown that the coefficients β_{ij} related to the phasor components $c_{k,r}$ and $s_{k,r}$, $k = 0, 1, 2,$ multiplying the real or imaginary parts of $X_{w2}^{(i)}(\nu_0)$ in (25) depend on $1/M^{(k+i)}$. Since $X_{w2}^{(i)}(\nu_0)$ is proportional to M^i (see (B.9) in the Appendix B) it follows that the contributions $\beta_{lh} X_{w2}^{(i)}(\nu_0)$ to $c_{k,r}$ and $s_{k,r}$, $k = 0, 1, 2,$ depend on $1/M^k$.

As a consequence of the previous analysis, only six different matrix elements, i.e. β_{11}, β_{13}, β_{15}, β_{22}, β_{24}, and β_{33}, are needed for estimating the phasor parameters when λ_0 is greater than about 3 bins. In that case (25) becomes:

$$\begin{aligned}
\hat{p}_{0,r} &= \hat{c}_{0,r} + j\hat{s}_{0,r} \cong \beta_{33} X_{W_2}(\nu_0) - \frac{\beta_{24}}{2\pi} X_{W_2}^{*(1)}(\nu_0) - \frac{\beta_{13}}{4\pi^2} X_{W_2}^{(2)}(\nu_0), \\
\hat{p}_{1,r} &= \hat{c}_{1,r} + j\hat{s}_{1,r} \cong -j\beta_{24} X_{W_2}^{*}(\nu_0) + j\frac{\beta_{22}}{2\pi} X_{W_2}^{(1)}(\nu_0) + j\frac{\beta_{15}}{4\pi^2} X_{W_2}^{*(2)}(\nu_0), \\
\hat{p}_{2,r} &= \hat{c}_{2,r} + j\hat{s}_{2,r} \cong \beta_{13} X_{W_2}(\nu_0) - \frac{\beta_{15}}{2\pi} X_{W_2}^{*(1)}(\nu_0) - \frac{\beta_{11}}{4\pi^2} X_{W_2}^{(2)}(\nu_0),
\end{aligned} \tag{26}$$

which expresses the relationships between the TWLS estimator and the analyzed waveform DTFT in a quite simple way.

The dynamic phasor parameter estimator based on expressions (26) will be called the Simplified TWLS (STWLS) procedure in the following.

IV. ACCURACY ASSESSMENT OF THE STWLS PROCEDURE

This Section is organized in three different subsections. The first one is aimed at verifying if the phasor parameter estimates returned by both the proposed TWLS and STWLS procedures comply with the requirements of the *M-class* of performance when the waveform frequency is a-priori estimated by the IpDFT method, i.e. when the TWLS-IpDFT or the STWLS-IpDFT procedures are used, respectively. Then, the accuracy that can be achieved by evaluating the coefficients $\beta_{lh}(\nu)$ by means of polynomials with low degree is analyzed. Finally, the computational burden required by the considered TWLS procedures is discussed in the last subsection.

A. *Compliance to Standard requirements of the TWLS-IpDFT and the STWLS-IpDFT procedures*

In this subsection the compliance to the requirements of the *M-class* of performance is checked for the phasor parameter estimates returned by both proposed procedures when the reference frequency is estimated run-time by the IpDFT algorithm [17] under steady-state, dynamic, and transients conditions specified in the Standard.

The worst-case off-nominal frequency, 2nd harmonic, 3rd harmonic, amplitude modulation (AM) and phase modulation (PM) testing conditions specified in the Standard for the *M-class* of performance are considered in Table I. Also, the related threshold values specified in the Standard are reported for comparison. The Hann window is adopted, $N = 24$ sample/cycle, $J = 3$, 4, 5, and 6 cycles, and the Taylor's series order is $K = 2$. The maximum values of the considered accuracy parameters were determined considering 960 subsequent records (corresponding to 40 nominal cycles of the analyzed waveform) shifted each other sample by sample. For each estimated parameter, the results returned by the proposed TWLS estimator (25) and the STWLS estimator (26) are reported in Table I.

As expected, the results reported in Table I show that the STWLS procedure can be as accurate as the TWLS procedure when a sufficient number of waveform cycles are observed. In particular, the STWLS procedure returns phasor parameter estimates compliant with the Standard requirements as soon as $J \geq 5$ in the off-nominal and 2nd harmonic testing, and when $J \geq 3$ in the 3rd harmonic and modulation testing.

Table I. Maximum magnitude of the *TVE*, *FE*, and *RFE* values returned by the proposed TWLS estimator (25) and the STWLS estimator (26) when the reference frequency f_0 is estimated run-time by the IpDFT algorithm. The Hann window is adopted and J = 3, 4, 5, and 6 cycles. The worst-case testing conditions specified in the Standard for the *M-class* of performance are considered.

Test type	J [cycle]	TVE_{max} [%]		FE_{max} [mHz]		RFE_{max} [Hz/s]	
		eq. (25)	eq. (26)	eq. (25)	eq. (26)	eq. (25)	eq. (26)
off-nominal frequency	3	0.00	0.44	0.00	2.62	0.00	11.0
	4	0.00	0.09	0.00	0.05	0.00	1.23
	5	0.00	0.01	0.00	0.01	0.00	0.10
	6	0.00	0.00	0.00	0.00	0.00	0.02
Standard threshold	—	1		5		0.1	
2nd harmonic	3	1.21	1.33	72.1	72.1	53.3	55.3
	4	0.13	0.15	8.80	8.86	3.14	3.45
	5	0.03	0.03	2.01	2.02	0.43	0.48
	6	0.01	0.01	0.63	0.63	0.09	0.10
3rd harmonic	3	0.01	0.17	1.28	3.10	0.36	3.93
	4	0.00	0.03	0.21	0.28	0.03	0.36
	5	0.00	0.01	0.05	0.06	0.01	0.06
	6	0.00	0.00	0.02	0.02	0.00	0.01
Standard threshold	—	1		5[(1)]-25[(2)]		—	
amplitude modulation	3	0.00	0.17	0.81	2.52	0.02	3.98
	4	0.01	0.04	1.81	1.77	0.02	0.41
	5	0.04	0.04	3.30	3.28	0.03	0.07
	6	0.07	0.07	5.25	5.24	0.05	0.05
phase modulation	3	0.00	0.18	15.3	17.3	0.44	4.52
	4	0.01	0.04	26.9	26.9	0.75	1.14
	5	0.03	0.04	41.5	41.5	1.16	1.23
	6	0.07	0.07	58.8	58.8	1.65	1.66
Std. thresh.	—	3		300		14	

Note: Threshold values are related to a Reporting Rate RR ≤ 20 [(1)] or RR > 20 [(2)].

It is worth noticing that the results related to the frequency ramp testing are almost equal to those related to the off-nominal frequency testing, while the results obtained when the analyzed waveform is affected by harmonics decreases as harmonic order increases.

The most severe testing condition related to the *M-class* of performance is the out-of-band interference. It is known that the GTWLS-IpDFT algorithm provides phasor parameter estimates compliant

with the Standard requirements when the Reporting Rate (RR) is equal to 50 readings/s only when $J \geq 8$ cycles [17]. The maximum TVE, FE, and RFE estimates returned by both procedures when the analyzed waveform is affected by out-of-band interference, $J = 8$ and 9 cycles and the RR = 50 readings/s. The worst case testing conditions are considered, i.e. $f_{in} = 47.5$ Hz with interfering frequency $f_{ih} = 25$ Hz and $f_{in} = 52.5$ Hz with $f_{ih} = 75$ Hz. The results obtained when the original waveform is analyzed or the interference is removed from that waveform after the estimation of its parameters by the IpDFT method are reported in Table II.

Table II. Out-of-band interference: maximum magnitude of the *TVE*, *FE*, and *RFE* values returned by the TWLS estimator (25) and the STWLS estimator (26) when reference frequency f_0 is estimated run-time by the IpDFT algorithm. The Hann window is adopted and $J = 8$ and 9 cycles. The worst-case testing conditions specified in the Standard for the *M-class* of performance when RR = 50 readings/s are considered.

Test parameters	***J*** [cycle]	TVE_{max} [%]		FE_{max} [mHz]		RFE_{max} [Hz/s]	
		eq. (25)	eq. (26)	eq. (25)	eq. (26)	eq. (25)	eq. (26)
$f_{in} = 47.5$ Hz, $f_{ih} = 25$ Hz	8	0.02	0.02	6.72	6.72	0.33	0.33
	9	0.13	0.13	3.37	3.37	0.62	0.63
$f_{in} = 47.5$ Hz, $f_{ih} = 25$ Hz[(1)]	8	0.39	0.39	7.63	7.63	1.35	1.35
	9	0.01	0.01	1.25	1.25	0.03	0.03
$f_{in} = 52.5$ Hz, $f_{ih} = 75$ Hz	8	0.02	0.02	6.72	6.72	0.32	0.32
	9	0.12	0.12	3.36	3.36	0.62	0.62
$f_{in} = 52.5$ Hz, $f_{ih} = 75$ Hz[(1)]	8	0.38	0.38	7.52	7.52	1.33	1.33
	9	0.01	0.01	1.22	1.22	0.03	0.03
Standard threshold	—	1.3		10		—	

Note: [(1)] Out-of-band interference removed from the analyzed waveform

As expected, when considering the same testing conditions, both procedures return very close results and they comply with the Standard requirements as soon as $J \geq 8$ cycles. It is worth emphasizing that the out-of-band interference removal when $J = 8$ results in worse estimates. This happens because of the poor parameter estimation performed by the IpDFT method due to the significant spectral interference from the fundamental component. That phenomenon does not occur when $J = 9$, since the interference parameters are accurately estimated.

The performances of the proposed procedures has been assessed also under transient conditions specified in the Standard. The results obtained when using RR = 50 readings/s are reported in Table III.

Table III. Waveform amplitude or phase step: absolute value of the worst-case overshoot or undershoot, and phasor, frequency, and *ROCOF* response times returned by the TWLS estimator (25) and the STWLS estimator (26) when the reference frequency f_0 is estimated run-time by the IpDFT algorithm. The Hann window is adopted and J = 3, 4, 5, and 6 cycles.

Test type	*J* *[cycles]*	*Overshoot (undershoot)* [%]		*Phasor response time* [nominal cycles]		*Frequency response time* [nominal cycles]		*ROCOF response time* [nominal cycles]	
		eq. (25)	eq. (26)	eq. (25)	eq. (26)	eq. (25)	eq. (26)	eq. (25)	eq. (26)
amplitude step	3	0.6	0.5	0.8	0.8	2.3	2.3	2.63	11.5
	4	0.5	0.5	0.9	0.9	2.9	2.9	3.42	12.0
	5	0.5	0.5	1.1	1.1	3.5	3.5	4.17	4.13
	6	0.5	0.5	1.3	1.3	4.1	4.1	4.92	4.92
phase step	3	5.4	5.6	0.9	0.9	2.5	2.5	2.71	11.5
	4	4.9	4.8	1.1	1.1	3.2	3.2	3.54	12.0
	5	4.7	4.7	1.3	1.3	4.0	4.0	4.38	4.38
	6	4.6	4.6	1.5	1.5	4.7	4.7	5.21	5.21
Std. thresh.	-	10		7[(1)]		14[(1)]		14[(1)]	

Note: [(1)] Threshold values are related to RR = 50.

Moreover, the delay times related to amplitude and phase steps have also been determined. The maximum delay time returned by simulations was equal to 1.67 ms when J = 5 or 6 cycles in the case of amplitude step, and to 2.5 ms for all considered values of J when phase step occurs. In any case the obtained delay times were significantly smaller than the upper threshold of 5 ms specified in the Standard for RR = 50 readings/s.

Simulations show that both procedures exhibit almost the same performances when $J \geq 3$ cycles, except for the ROCOF response time where the same value is achieved only for $J \geq 5$ cycles. However, both procedures comply with the Standard requirements in all the considered testing conditions.

It is worth noticing that for J = 8 and 9 the maximum TVE, FE, and RFE estimates provided by both the considered procedures under the off-nominal frequency, harmonics, AM, PM, and frequency ramp testing conditions comply with the Standard requirements. In particular, negligible estimation errors are obtained in the case of off-nominal frequency and harmonics testing.

B. *Polynomial approximation of the β_{lh} coefficients used by the STWLS procedure*

In order to further lower down the computing complexity required when implementing the TWLS algorithm (25) or (26), the coefficients $\beta_{lh}(\nu)$ have been approximated by means of a least squares polynomial fitting in the whole frequency range specified in the Standard for the *M-class* of performance,

i.e. considering a worst-case off-nominal frequency of 5 Hz. In that way, the phasor parameter estimation can be implemented in real-time on low-cost hardware platforms even though the analyzed waveform frequency is determined run-time to improve the phasor estimation accuracy. The value of the expression $\underset{l,h}{w.c.}\max_{\nu}\left|\left(\hat{\beta}_{lh}(\nu)-\beta_{lh}(\nu)\right)/\beta_{lh}(\nu_0)\right|$%, i.e. the worst-case with respect to all the significant coefficients of the maximum in the considered frequency range of the magnitude of the ratio between the approximation error and the value $\beta_{lh}(\nu_0)$ of the related coefficient at the nominal frequency, is reported in Table IV as a function of the approximating polynomial degree and J = 2, 4, and 6 nominal cycles. It is worth noticing that even polynomials of low degree provide acceptable or negligible value for the maximum relative worst-case error.

Table IV: Worst-case of the maximum relative polynomial approximation error of the coefficients β_{lh} for different values of M and polynomial degrees. The Hann window is adopted, N = 24 sample per cycle and the worst-case off-nominal frequency is 5 Hz.

J [cycle]	polyn. degree 5	polyn. degree 6	polyn. degree 7
2	0.33%	$3.9\cdot10^{-4}$%	$4.2\cdot10^{-5}$%
4	2.0%	0.49%	$8.6\cdot10^{-4}$%
6	9.9%	6.1%	0.52%

Table V shows the accuracy (expressed in terms of *TVE*, *FE*, and *RFE*) provided by the TWLS algorithm when the waveform is affected by off-nominal frequency up to 5 Hz and J = 2, 4, or 6 nominal cycles are observed. Different implementations of the TWLS estimator are considered, that is: the classical algorithm based on the waveform nominal frequency, expressions (25) and (26) based on the true waveform frequency with coefficients β_{lh} evaluated at run-time using exact expression or polynomials of degree 3 or 5, respectively.

The accuracy of the TWLS algorithm reported in the first column of Table V is related to the most efficient implementation in terms of computational effort, i.e., by assuming the nominal waveform frequency so that the matrix B_K^{-1} can be computed offline. Compared to such an implementation, Table V clearly shows how the approximation (26) has the main detrimental effect for the frequency estimates. Moreover, for J = 2 cycles, it returns low accuracy results even if the exact coefficients are considered. A radically different behavior is instead achieved when J = 4 cycles, where the accuracies of (25) and (26) are very close, apart again from the frequency estimates. For J = 6 cycles both (25) and (26) provide highly accurate results for all the estimated parameters. To summarize, the polynomial approximation of (25)

always returns better results than the TWLS algorithm at the nominal frequency but at the cost of an increased computational effort. To reduce that effort, expressions (26) can be used, which are very effective if at least 4 waveform cycles are observed. Not surprisingly, the accuracy obtained by both (25) and (26) scales with the degree of the approximating polynomial and, hence, with the needed computation effort, but with a lower extent than the number of observed waveform cycles.

Table V: Maximum magnitude of the *TVE*, *FE* and *RFE* values returned by different implementations of the TWLS estimator when the off-nominal frequency testing specified in the Standard for the *M-class* of performance is considered. The Hann window is adopted and $N = 24$ sample/cycle.

		TWLS at nominal freq	TWLS based on (25)			STWLS based on (26)		
J [cycle]	Phasor parameters		exact coeff.	pol. deg. 3	pol. deg. 5	exact coeff.	pol. deg. 3	pol. deg. 5
2	TVE_{max} [%]	$7 \cdot 10^{-2}$	$2.7 \cdot 10^{-13}$	$7.5 \cdot 10^{-2}$	$2.0 \cdot 10^{-3}$	$1.1 \cdot 10^{-1}$	$1.8 \cdot 10^{-2}$	$1.1 \cdot 10^{-2}$
	FE_{max} [mHz]	77.4	$2.5 \cdot 10^{-11}$	14	$4.9 \cdot 10^{-2}$	279	279	279
	RFE_{max} [Hz/s]	5.1	$8.6 \cdot 10^{-12}$	2.7	$8.0 \cdot 10^{-2}$	3.1	5.7	3.2
4	TVE_{max} [%]	$1.4 \cdot 10^{-1}$	$3.6 \cdot 10^{-13}$	$7.3 \cdot 10^{-3}$	$4.8 \cdot 10^{-4}$	$1.8 \cdot 10^{-5}$	$7.3 \cdot 10^{-3}$	$4.8 \cdot 10^{-4}$
	FE_{max} [mHz]	269	$2.3 \cdot 10^{-11}$	$4.0 \cdot 10^{-1}$	$8.8 \cdot 10^{-3}$	2.3	2.3	2.3
	RFE_{max} [Hz/s]	$1.1 \cdot 10^{-1}$	$2.9 \cdot 10^{-12}$	$2.0 \cdot 10^{-1}$	$1.3 \cdot 10^{-2}$	$3.3 \cdot 10^{-5}$	$2 \cdot 10^{-1}$	$1.3 \cdot 10^{-2}$
6	TVE_{max} [%]	$6.5 \cdot 10^{-1}$	$3.5 \cdot 10^{-13}$	$2.7 \cdot 10^{-3}$	$4.8 \cdot 10^{-4}$	$5.9 \cdot 10^{-7}$	$2.7 \cdot 10^{-3}$	$4.8 \cdot 10^{-4}$
	FE_{max} [mHz]	566	$2.1 \cdot 10^{-11}$	$1.6 \cdot 10^{-1}$	$2.1 \cdot 10^{-2}$	$2.8 \cdot 10^{-1}$	$2.8 \cdot 10^{-1}$	$2.8 \cdot 10^{-1}$
	RFE_{max} [Hz/s]	$3.4 \cdot 10^{-2}$	$1.3 \cdot 10^{-12}$	$3.4 \cdot 10^{-2}$	$6.1 \cdot 10^{-3}$	$5.1 \cdot 10^{-7}$	$3.4 \cdot 10^{-2}$	$6.1 \cdot 10^{-3}$

C. *Computational burden*

In this section, the computational burdens requested by the different implementations of the real-valued TWLS phasor parameter estimator proposed in the paper are compared each other. To this aim it is worth noticing that the procedure (10) requests a pseudoinverse computation, whose complexity varies according to the adopted algorithm (e.g., the Greville's method, the Singular Value Decomposition, the full rank QR factorization, optimized iterative methods). However, since the matrix WU_K has a particular structure (see (B.16) for $K = 2$), the pseudoinverse computation is less than $O(M^2 (2K+2))$ needed, for example, by the Singular Values method, as also reported in [25]. In practice, the complexity required for the pseudoinverse is slightly higher than computing explicitly the $\beta_{lh}(\nu)$ in (B.19) and then applying expression (25). For example, on a standard Laptop equipped with a 2.8 GHz Intel Core i7 with 16 GB of RAM and Yosemite OsX running Matlab, the mean time is 59.3 μs for pseudo-inverse computation and it is 56.2 μs when (25) is applied; in both situations the sample standard deviation of observations is about 8 μs.

As a consequence, in the following we compare the computational burden required by the approximated solution (26) only with the expression (25). Both methods comprise the explicit computation of $X_{w2}^{(k)}(\nu)$, which can then be neglected in the comparison. Considering $K = 2$ and assuming that the terms $n^h w^2(n)$ in (B.17) are pre-computed and stored in memory, the computational complexity of (B.17) amounts to $14 \cdot M$ products and $8 \cdot M$ sums. Then, the evaluation of the $\beta_{lh}(\nu)$ coefficients in (B.19) needs 56 products and 20 sums, while the final estimates (25) require additional 18 products and 12 sums. To summarize, the procedure (25) requires $74 + 14 \cdot M$ products and $32 + 8 \cdot M$ sums. On the other hand, the adoption of (26) with an approximant polynomial of degree 7 asks for 6 products and 7 sums for the $\beta_{lh}(\nu)$ approximants. Noticing that (26) makes use of only eight $\beta_{lh}(\nu)$ values, and hence asks for 10 products and 4 sums, the related overall computational complexity is 58 products and 60 sums, far less than the one required when (25) is adopted.

V. CONCLUSIONS

In this paper the analytical relationship between the phasor parameter estimates returned by the TWLS approach, expressed using either complex-valued or real-valued variables, has been derived. It has been shown that the TWLS phasor estimator and its derivatives can be expressed as weighted summations of the DTFT of the analyzed waveform and its derivatives. The analyzed waveform is weighted by the square of the window adopted in the WLS problem, while the weights used in the summation depend on the DTFT of the square window and its derivatives. As a consequence, the TWLS algorithm is sensitive to lower order harmonics and inter-harmonics located close to the waveform frequency when few waveform cycles are analyzed. In particular, phasor estimation errors due to harmonics are not null even though coherent sampling occurs because of the contribution of window spectrum derivatives. Also, windows squaring and derivation of waveform transform increase the sensitivity of the TWLS algorithm to wideband noise.

In addition, the relationship between the TWLS phasor estimator and the waveform DTFT has been specifically analyzed when either a static phasor model (i.e. the Taylor's series order is zero) or a second-order dynamic phasor model (i.e. the Taylor's series order is equal to two) is considered. This latter model is often adopted in the literature since it allows the estimation of the waveform phasor, frequency, and ROCOF while exhibiting acceptable computational effort and disturbance sensitivity. Using the derived expressions a procedure for the implementation of the TWLS algorithm without the calculation of the pseudoinverse matrix has been proposed. Furthermore, the expressions related to the second-order dynamic phasor model and the real-valued version of the TWLS algorithm have been approximated in order to

reduce the required computational effort and the STWLS procedure has been proposed. It has been shown by means of computer simulations that the phasor parameter estimates returned by the STWLS procedure when the waveform frequency is estimated by the IpDFT method comply with the *M-class* of performance if the number of analyzed waveform cycles is properly chosen. Moreover, the coefficients involved in the STWLS procedure can be evaluated by means of simple polynomials with high accuracy. Due to its lower computational complexity, the proposed STWLS-IpDFT procedure can be advantageously implemented in real-time low-*cost* measurement units.

Appendix A
Equivalence between the complex and real TWLS

Assume that $\hat{P}_{K,r}^{(C)}$ is the solution of the complex-valued TWLS algorithm, as reported in (4). Hence, for any nonsingular matrix $T \in R^{2(K+1)\times 2(K+1)}$ we have:

$$A_K \hat{P}_{K,r}^{(C)} = C_K x_r, \quad \text{or} \quad TA_K T^{-1} T\hat{P}_{K,r}^{(C)} = TC_K x_r, \tag{A.1}$$

for r = 0,1, 2, …. Let us consider the following choice:

$$T = \frac{1}{2}\begin{bmatrix} I_{K+1} & \bar{I}_{K+1} \\ jI_{K+1} & -j\bar{I}_{K+1} \end{bmatrix} \text{ and } T^{-1} = \begin{bmatrix} I_{K+1} & -j\bar{I}_{K+1} \\ \bar{I}_{K+1} & jI_{K+1} \end{bmatrix}, \tag{A.2}$$

where I_{K+1} is the identity matrix of dimension *K+1*, while $\bar{I}_{K+1}$ is the *anti-diagonal identity matrix* of dimension K +1, i.e., a matrix filled with zeros and having all the elements of its anti-diagonal equal to one. As a consequence, the matrix T expresses a linear combination of two terms at a time. With such a choice, by simple algebraic manipulations immediately follows that $Q_K T^{-1} = 2U_K$ and $TQ_K^H = U_K^T$, where the matrices are defined in (6) and (12).

Recalling (4) we have: $TA_K T^{-1} = \frac{1}{2} TQ_K^H W^H W Q_K T^{-1} = U_K^T W^T W U_K = B_K$, where B_K is defined in (10). Moreover, considering again (10), we obtain: $TC_K = TQ_K^H W^H W = U_K^T W^T W = D_K$. Substituting the last two equations into (A.1), we achieve: $B_K T\hat{P}_{K,r}^{(C)} = D_K x_r$. Since by the choice of T made so far it follows that $T\hat{P}_{K,r}^{(C)} = \hat{P}_{K,r}^{(R)}$, the equivalence between the real-valued and the complex-valued approaches follows.

A major consequence of the equivalence is the simplification of the complex-valued TWLS solution computation, which involves the inversion of the complex matrix A_K. Indeed, inverting B_K (or, even,

approximate it using polynomials) is much less computational demanding. The inverse matrix of A_K is then obtain by $A_K^{-1} = T^{-1} B_K^{-1} T$.

Appendix B

Derivation of the relationship between the TWLS and the DTFT phasor estimators

Let us consider the matrix $B_K = U_K^T W^T W U_K$ employed in the real-valued TWLS phasor estimation approach. After some algebra we can write:

$$B_K = \begin{bmatrix} B_{K,1} & B_{K,3} \\ B_{K,2} & B_{K,4} \end{bmatrix}, \tag{B.1}$$

whose entries are given by:

$$\begin{aligned}
(b_{K,1})_{lh} &= CC_{2K+2-l-h}(\nu_0), \quad l = 1,2,\ldots,K+1, \; h = 1,2,\ldots,K+1 \\
(b_{K,2})_{lh} &= CS_{K+l-h}(\nu_0), \qquad l = 1,2,\ldots,K+1, \; h = 1,2,\ldots,K+1 \\
(b_{K,3})_{lh} &= CS_{K-l+h}(\nu_0), \qquad l = 1,2,\ldots,K+1, \; h = 1,2,\ldots,K+1 \\
(b_{K,4})_{lh} &= SS_{l+h-2}(\nu_0), \qquad l = 1,2,\ldots,K+1, \; h = 1,2,\ldots,K+1,
\end{aligned} \tag{B.2}$$

where $\nu_0 = f_0/f_s$ and:

$$\begin{aligned}
CC_k(\nu) &= \sum_{n=-N_H}^{N_H} n^k w^2(n) \cos^2(2\pi\nu n), \\
SS_k(\nu) &= \sum_{n=-N_H}^{N_H} n^k w^2(n) \sin^2(2\pi\nu n), \\
CS_k(\nu) &= \sum_{n=-N_H}^{N_H} n^k w^2(n) \cos(2\pi\nu n) \sin(2\pi\nu n).
\end{aligned} \tag{B.3}$$

This expression shows that CC_k and SS_k are nulls if k is odd, while CS_k is null if k is even. Thus, the entries of the matrix B can be expressed as:

$$(b_{K,1})_{lh} = \begin{cases} 0.5\left(\frac{j}{2\pi}\right)^{2K+2-l-h} M[W_2^{(2K+2-l-h)}(0) + W_2^{(2K+2-l-h)}(2\nu_0)], & \text{if} \quad 2K+2-l-h \ \text{is even} \\ 0 & \text{if} \quad 2K+2-l-h \ \text{is odd} \end{cases}$$

$$(b_{K,2})_{lh} = \begin{cases} 0.5j\left(\frac{j}{2\pi}\right)^{K+1+l-h} M \cdot W_2^{(K+l-h)}(2\nu_0), & \text{if} \quad K+l-h \quad \text{is odd} \\ 0 & \text{if} \quad K+l-h \quad \text{is even} \end{cases} \tag{B.4}$$

$$(b_{K,3})_{lh} = \begin{cases} 0.5j\left(\frac{j}{2\pi}\right)^{K+1-l+h} M \cdot W_2^{(K-l+h)}(2\nu_0), & \text{if} \quad K-l+h \quad \text{is odd} \\ 0 & \text{if} \quad K-l+h \quad \text{is even} \end{cases}$$

$$(b_{K,4})_{lh} = \begin{cases} 0.5\left(\frac{j}{2\pi}\right)^{l+h-2} M[W_2^{(l+h-2)}(0) - W_2^{(l+h-2)}(2\nu_0)], & \text{if} \quad l+h-2 \quad \text{is even} \\ 0 & \text{if} \quad l+h-2 \quad \text{is odd} \end{cases}$$

$$l = 1, 2, \ldots, K+1, \ \ h = 1, 2, \ldots, K+1.$$

where:

$$W_2(\nu) = \frac{1}{M} \sum_{n=-N_H}^{N_H} w^2(n) e^{-j2\pi\nu n}. \tag{B.5}$$

is the DTFT of the square window $w^2(\cdot)$ and:

$$W_2^{(k)}(\nu) = \frac{d^k W_2(\nu)}{d\nu^k} = \frac{1}{M}(-j2\pi)^k \sum_{n=-N_H}^{N_H} n^k w^2(n) e^{-j2\pi\nu n} \tag{B.6}$$

is the *k*-order derivative of the $W_2(\cdot)$. It is worth noticing that $W_2^{(k)}(\cdot)$ is an even or odd function of its argument when *k* is even or odd, respectively. Moreover, $W_2^{(k)}(0)$ is null when *k* is odd.

Moreover, after some algebra we obtain:

$$U_K^H W^H W\, x = \begin{bmatrix} \sum_{n=-N_H}^{N_H} n^K x(n)\, w^2(n) \cos(2\pi\nu_0 n) \\ \sum_{n=-N_H}^{N_H} n^{K-1} x(n)\, w^2(n) \cos(2\pi\nu_0 n) \\ \vdots \\ \sum_{n=-N_H}^{N_H} x(n)\, w^2(n) \cos(2\pi\nu_0 n) \\ \sum_{n=-N_H}^{N_H} x(n)\, w^2(n) \sin(2\pi\nu_0 n) \\ \vdots \\ \sum_{n=-N_H}^{N_H} n^{K-1} x(n)\, w^2(n) \sin(2\pi\nu_0 n) \\ \sum_{n=-N_H}^{N_H} n^K x(n)\, w^2(n) \sin(2\pi\nu_0 n) \end{bmatrix} = M \times \begin{bmatrix} \mathrm{Re}\left\{\left(\frac{j}{2\pi}\right)^K X_{W_2}^{(K)}(\nu_0)\right\} \\ \mathrm{Re}\left\{\left(\frac{j}{2\pi}\right)^{K-1} X_{W_2}^{(K-1)}(\nu_0)\right\} \\ \vdots \\ \mathrm{Re}\{X_{W_2}(\nu_0)\} \\ -\mathrm{Im}\{X_{W_2}(\nu_0)\} \\ \vdots \\ -\mathrm{Im}\left\{\left(\frac{j}{2\pi}\right)^{K-1} X_{W_2}^{(K-1)}(\nu_0)\right\} \\ -\mathrm{Im}\left\{\left(\frac{j}{2\pi}\right)^{K} X_{W_2}^{(K)}(\nu_0)\right\} \end{bmatrix}, \tag{B.7}$$

where:

$$X_{W2}(\nu) = \frac{1}{M} \sum_{n=-N_H}^{N_H} x(n) w^2(n) e^{-j2\pi\nu n}, \tag{B.8}$$

is the DTFT of the analyzed waveform weighted by the square window $w^2(\cdot)$ and

$$X_{W2}^{(k)}(\nu) = \frac{d^k X_{W2}(\nu)}{d\nu^k} = \frac{1}{M}(-j2\pi)^k \sum_{n=-N_H}^{N_H} n^k x(n)\, w^2(n) e^{-j2\pi\nu n}, \tag{B.9}$$

is its k-order derivative.

By denoting the entries of the matrix B_K^{-1} with β_{lh}, $l, h = 1, 2, \ldots, 2K + 2$, from (11) and (B.9) it follows:

$$\hat{c}_{K-k,r} = \sum_{l=1}^{K+1} \beta_{(k+1)l}\, \mathrm{Re}\left\{\left(\frac{j}{2\pi}\right)^{K+1-l} X_{W_2}^{(K+1-l)}(\nu_0)\right\} - \sum_{l=1}^{K+1} \beta_{(k+1)(2K+3-l)}\, \mathrm{Im}\left\{\left(\frac{j}{2\pi}\right)^{K+1-l} X_{W_2}^{(K+1-l)}(\nu_0)\right\}, \tag{B.10.a}$$

$$k = 0,1,\ldots,K$$

and

$$\hat{s}_{K-k,r} = -\sum_{l=1}^{K+1} \beta_{(2K+2-k)l}\, \mathrm{Re}\left\{\left(\frac{j}{2\pi}\right)^{K+1-l} X_{W_2}^{(K+1-l)}(\nu_0)\right\} \tag{B.10.b}$$

$$+ \sum_{l=1}^{K+1} \beta_{(2K+2-k)(2K+3-l)}\, \mathrm{Im}\left\{\left(\frac{j}{2\pi}\right)^{K+1-l} X_{W_2}^{(K+1-l)}(\nu_0)\right\}, \qquad k = 0,1,\ldots,K$$

Finally, expression (21) easily follows from (B.10.a) and (B.10.b).

A. *Static phasor model* ($K = 0$)

When $K = 0$, the relationship between the TWLS and the DTFT phasor estimators can be easily achieved not only from the expressions above, but also directly from (4). Indeed, in this case the matrix A_0 has the following expression:

$$A_0 = \frac{1}{2} Q_0^H W^H W Q_0 = \frac{M}{2} \times \begin{bmatrix} W_2(0) & W_2(2\nu_0) \\ W_2(2\nu_0) & W_2(0) \end{bmatrix} \tag{B.11}$$

From (B.11) it is easy to obtain:

$$A_0^{-1} = \frac{2}{M} \frac{1}{W_2^2(0) - W_2^2(2\nu_0)} \begin{bmatrix} W_2(0) & -W_2(2\nu_0) \\ -W_2(2\nu_0) & W_2(0) \end{bmatrix} \tag{B.12}$$

Moreover, in (4):

$$C_0 x_r = Q_0^H W^H W x_r = M \times \begin{bmatrix} X_{W_2}(\nu_0) \\ X_{W_2}^*(\nu_0) \end{bmatrix}. \tag{B.13}$$

By substituting (B.12) and (B.13) in (4) it follows that:

$$\hat{P}_{0,r} = A_0^{-1} C_0 x_r = \frac{2}{W_2^2(0) - W_2^2(2\nu_0)} \begin{bmatrix} W_2(0) X_{W_2}(\nu_0) - W_2(2\nu_0) X_{W_2}^*(\nu_0) \\ W_2(0) X_{W_2}^*(\nu_0) - W_2(2\nu_0) X_{W_2}(\nu_0) \end{bmatrix}, \tag{B.14}$$

from which, using (5):

$$\hat{p}_{0,r} = 2 \frac{W_2(0) X_{W_2}(\nu_0) - W_2(2\nu_0) X_{W_2}^*(\nu_0)}{W_2^2(0) - W_2^2(2\nu_0)}. \tag{B.15}$$

The same result can be achieved using the real-valued TWLS phasor estimator approach, i.e. using (10) and (11).

B. *Second order dynamic phasor model* ($K = 2$)

From (B.2) and (B.3) it follows that the matrix B_2 can be expressed as:

$$B_2 = \begin{bmatrix} a_4 & 0 & a_2 & 0 & c_3 & 0 \\ 0 & a_2 & 0 & c_1 & 0 & c_3 \\ a_2 & 0 & a_0 & 0 & c_1 & 0 \\ 0 & c_1 & 0 & b_0 & 0 & b_2 \\ c_3 & 0 & c_1 & 0 & b_2 & 0 \\ 0 & c_3 & 0 & b_2 & 0 & b_4 \end{bmatrix}, \tag{B.16}$$

where:

$$
\begin{aligned}
a_0 &\overset{\Delta}{=} CC_0(\nu_0) = \sum_{n=-N_H}^{N_H} w^2(n)\cos^2(2\pi\nu_0 n),\\
a_2 &\overset{\Delta}{=} CC_2(\nu_0) = \sum_{n=-N_H}^{N_H} n^2 w^2(n)\cos^2(2\pi\nu_0 n),\\
a_4 &\overset{\Delta}{=} CC_4(\nu_0) = \sum_{n=-N_H}^{N_H} n^4 w^2(n)\cos^2(2\pi\nu_0 n),\\
b_0 &\overset{\Delta}{=} SS_0(\nu_0) = \sum_{n=-N_H}^{N_H} w^2(n)\sin^2(2\pi\nu_0 n),\\
b_2 &\overset{\Delta}{=} SS_2(\nu_0) = \sum_{n=-N_H}^{N_H} n^2 w^2(n)\sin^2(2\pi\nu_0 n),\\
b_4 &\overset{\Delta}{=} SS_4(\nu_0) = \sum_{n=-N_H}^{N_H} n^4 w^2(n)\sin^2(2\pi\nu_0 n),\\
c_1 &\overset{\Delta}{=} CS_1(\nu_0) = 0.5\sum_{n=-N_H}^{N_H} n w^2(n)\sin(4\pi\nu_0 n),\\
c_3 &\overset{\Delta}{=} CS_3(\nu_0) = 0.5\sum_{n=-N_H}^{N_H} n^3 w^2(n)\sin(4\pi\nu_0 n).
\end{aligned}
\tag{B.17}
$$

Moreover:

$$
B_2^{-1} = \frac{1}{M}\begin{bmatrix}
\beta_{11} & 0 & \beta_{13} & 0 & \beta_{15} & 0\\
0 & \beta_{22} & 0 & \beta_{24} & 0 & \beta_{26}\\
\beta_{13} & 0 & \beta_{33} & 0 & \beta_{35} & 0\\
0 & \beta_{24} & 0 & \beta_{44} & 0 & \beta_{46}\\
\beta_{15} & 0 & \beta_{35} & 0 & \beta_{55} & 0\\
0 & \beta_{26} & 0 & \beta_{46} & 0 & \beta_{66}
\end{bmatrix},
\tag{B.18}
$$

in which the expressions of the entries of the inverse matrix B^{-1} returned by the *Symbolic Math Toolbox* of MATLAB are:

$$
\begin{aligned}
\beta_{11} &= \ M(c_1^2 - a_0 b_2)/(a_4 c_1^2 - 2a_2 c_3 c_1 + b_2 a_2^2 + a_0 c_3^2 - a_0 b_2 a_4),\\
\beta_{13} &= -M(c_1 c_3 - a_2 b_2)/(a_4 c_1^2 - 2a_2 c_3 c_1 + b_2 a_2^2 + a_0 c_3^2 - a_0 b_2 a_4),\\
\beta_{15} &= -M(a_2 c_1 - c_3 a_0)/(a_4 c_1^2 - 2a_2 c_3 c_1 + b_2 a_2^2 + a_0 c_3^2 - a_0 b_2 a_4),\\
\beta_{22} &= -M(-b_2^2 + b_0 b_4)/(b_4 c_1^2 - 2b_2 c_3 c_1 + a_2 b_2^2 + b_0 c_3^2 - a_2 b_0 b_4),\\
\beta_{24} &= \ M(c_1 b_4 - c_3 b_2)/(b_4 c_1^2 - 2b_2 c_3 c_1 + a_2 b_2^2 + b_0 c_3^2 - a_2 b_0 b_4),\\
\beta_{26} &= -M(c_1 b_2 - b_0 c_3)/(b_4 c_1^2 - 2b_2 c_3 c_1 + a_2 b_2^2 + b_0 c_3^2 - a_2 b_0 b_4),\\
\beta_{33} &= -M(a_4 b_2 - c_3^2)/(a_4 c_1^2 - 2a_2 c_3 c_1 + b_2 a_2^2 + a_0 c_3^2 - a_0 b_2 a_4),\\
\beta_{35} &= \ M(a_4 c_1 - a_2 c_3)/(a_4 c_1^2 - 2a_2 c_3 c_1 + b_2 a_2^2 + a_0 c_3^2 - a_0 b_2 a_4),\\
\beta_{44} &= -M(a_2 b_4 - c_3^2)/(b_4 c_1^2 - 2b_2 c_3 c_1 + a_2 b_2^2 + b_0 c_3^2 - a_2 b_0 b_4),\\
\beta_{46} &= -M(c_1 c_3 - a_2 b_2)/(b_4 c_1^2 - 2b_2 c_3 c_1 + a_2 b_2^2 + b_0 c_3^2 - a_2 b_0 b_4),\\
\beta_{55} &= \ M(a_2^2 - a_0 a_4)/(a_4 c_1^2 - 2a_2 c_3 c_1 + b_2 a_2^2 + a_0 c_3^2 - a_0 b_2 a_4),\\
\beta_{66} &= \ M(c_1^2 - b_0 a_2)/(b_4 c_1^2 - 2b_2 c_3 c_1 + a_2 b_2^2 + b_0 c_3^2 - a_2 b_0 b_4).
\end{aligned}
\tag{B.19}
$$

Using (B.19), (B.10) provides the expressions (25) for the Taylor parameters estimates returned by the TWLS approach for $K = 2$.

REFERENCES

[1] *IEEE Standard C37.118.1 for Synchrophasor Measurements for Power Systems,* Dec. 2011.

[2] *Amendment 1: Modification of Selected Performance Requirements, to IEEE Standard C37.118.1-2011 for Synchrophasor Measurements for Power Systems, IEEE Standard C37.118.1a-2014*.

[3] A.G. Phadke and B. Kasztenny, "Synchronized phasor and frequency measurement under transient conditions," *IEEE Trans. Power Del.*, vol. 24, no. 1, pp. 89-95, Jan. 2009.

[4] W. Premerlani, B. Kasztenny, and M. Adamiak, "Development and implementation of a synchrophasor estimator capable of measurements under dynamic conditions," *IEEE Trans. Power Del.*, vol. 23, no. 1, pp. 109-123, Jan. 2008.

[5] J.A. de la O Serna, "Dynamic phasor estimates for power system oscillation," *IEEE Trans. Instrum. Meas.*, vol. 56, no. 5, pp. 1648-1657, Oct. 2007.

[6] M. Platas-Garza and J. de la O. Serna, "Dynamic phasor and frequency estimates through maximally flat differentiators," *IEEE Trans. Instrum. Meas.*, vol. 59, no. 7, pp. 1803-1811, Jul. 2010.

[7] A.J. Roscoe, I.F. Abdulhadi, and G.M. Burt, "P and M class phasor measurement unit algorithms using adaptive cascaded filters," *IEEE Trans. Power Del.*, vol. 28, no. 3, pp. 1447-1459, Jul. 2013.

[8] A.J. Roscoe, "Exploring the relative performance of frequency-tracking and fixed-filter phasor measurement unit algorithms under C37.118 test procedures, the effects of interharmonics, and initial attemps at merging P-class response with M-class filtering," *IEEE Trans. Instrum. Meas.*, vol. 62, no. 8, pp. 2140-2153, Aug. 2013.

[9] R.K. Mai, Z.Y. He, L.Fu, B. Kirby, and Z.Q. Bo, "A dynamic synchrophasor estimation algorithm for online application," *IEEE Trans. Power Del.*, vol. 25, no. 2, pp. 570-578, Apr. 2010.

[10] P. Castello, M. Lixia, C. Muscas, and P.A. Pegoraro, "Impact of the model on the accuracy of synchrophasor measurement," *IEEE Trans. Instrum. Meas.*, vol. 61, no. 8, pp. 2179-2188, Aug. 2012.

[11] P. Castello, L. Junqi, C. Muscas, P.A. Pegoraro, F. Ponci, and A. Monti, "A fast and accurate PMU algorithm for P+M class measurement of synchrophasor and frequency," *IEEE Trans. Instrum. Meas.*, vol. 63, no. 12, pp. 2837-2845, Dec. 2014.

[12] G. Barchi, D. Macii, and D. Petri "Synchrophasor estimators accuracy: A comparative analysis," *IEEE Trans. Instrum. Meas.*, vol. 62, no. 5, pp. 963-973, May 2013.

[13] D. Belega, D. Macii, and D. Petri, "Fast synchrophasor estimation by means of frequency-domain and time-domain algorithms," *IEEE Trans. Instrum. Meas.*, vol. 63, no. 2, pp. 388-401, Feb. 2014.

[14] D. Belega and D. Petri, "Dynamic synchrophasor estimation in the presence of the decaying dc offsets," in Proc. IEEE I2MTC Conference, pp. 502-507, Montevideo, Uruguay, May 2014.

[15] D. Petri, D. Fontanelli, and D. Macii, "A frequency-domain algorithm for dynamic synchrophasor and frequency estimation," *IEEE Trans. Instrum. Meas.*, vol. 63, no. 10, pp. 2330-2340, Oct. 2014.

[16] S. Das and T. Sidhu, "A simple synchrophasor estimation algorithm considering IEEE standard C37.118-2011 and protection requirements," *IEEE Trans. Instrum. Meas.*, vol. 62, no. 10, pp. 2704-2715, Oct. 2013.

[17] D. Belega, D. Fontanelli, and D. Petri, "Dynamic phasor and frequency measurements by an improved Taylor weighted least squares algorithm", *IEEE Trans. Instrum. Meas.*, in press.

[18] D. Macii, D. Petri, and A Zorat, "Accuracy analysis and enhancement of DFT-based synchrophasor estimators in off-nominal conditions," *IEEE Trans. Instrum. Meas.*,, vol. 61, no. 10, pp. 2653-2664, Oct. 2012.

[19] D. Belega and D. Petri "Accuracy analysis of the multicycle synchrophasor estimator provided by the interpolated DFT algorithm," *IEEE Trans. Instrum. Meas.*, 62, no. 5, pp. 942-953, May 2013.

[20] P. Romano and M. Paolone, "Enhanced interpolated-DFT for synchrophasor estimation in FPGAs: Theory, implementation, and validation of a PMU prototype," *IEEE Trans. Instrum. Meas.*, vol. 63, no. 12, pp. 2824-2836, Dec. 2014.

[21] D. Belega and D. Petri, "A real-valued Taylor weighted least squares synchrophasor estimator," in Proc. IEEE Int. Workshop on Applied Measurements for Power Systems (AMPS), pp. 1-6, Aachen, Germany, 24-26 Sept. 2014.

[22] A.H. Nuttall, "Some windows with very good sidelobe behavior," *IEEE Trans. Acoust., Speech, Signal Proces.*, vol. ASSP-29, no.1, pp 84–91, Feb. 1981.

[23] F.J. Harris, "On the use of windows for harmonic analysis with the discrete Fourier transform," *Proc. IEEE*, vol. 66, no.1, pp 51–83, Jan. 1978.

[24] IEEE Std. 1241, Standard for Terminology and Test Methods for Analog-to-Digital Converters, 2010.

[25] J.A. de la O Serna, "Synchrophasor Measurement With Polynomial Phase-Locked-Loop Taylor–Fourier Filters," *IEEE Trans. Instrum. Meas.*, vol. 64, no. 2, pp. 328-337, Feb. 2015.